HHS Public Access

Author manuscript

Alcohol. Author manuscript; available in PMC 2016 September 01.

Published in final edited form as:

Alcohol. 2015 September ; 49(6): 571–580. doi:10.1016/j.alcohol.2015.04.008.

Selective reduction of cerebral cortex GABA neurons in a late gestation model of fetal alcohol spectrum disorder

John F. Smiley[a,b], **Mariko Saito**[a,b], **Cynthia Bleiwas**[a], **Kurt Masiello**[a], **Babak Ardekani**[a], **David N. Guilfoyle**[a], **Scott Gerum**[a], **Donald A. Wilson**[a,c], and **Csaba Vadasz**[a,b]

[a]Nathan Kline Institute for Psychiatric Research, Orangeburg, NY, USA

[b]Department of Psychiatry, New York University Medical Center, New York, NY, USA

[c]Department of Child and Adolescent Psychiatry, New York University Medical Center, New York, NY, USA

Abstract

Fetal alcohol spectrum disorders (FASD) are associated with cognitive and behavioral deficits, and decreased volume of the whole brain and cerebral cortex. Rodent models have shown that early postnatal treatments, which mimic ethanol toxicity in the third trimester of human pregnancy, acutely induce widespread apoptotic neuronal degeneration and permanent behavioral deficits. However, the lasting cellular and anatomical effects of early ethanol treatments are still incompletely understood. This study examined changes in neocortex volume, thickness, and cellular organization that persist in adult mice after postnatal day 7 (P7) ethanol treatment. Post mortem brain volumes, measured by both MRI within the skull and by fluid displacement of isolated brains, were reduced 10–13% by ethanol treatment. The cerebral cortex showed a similar reduction (12%) caused mainly by lower surface area (9%). In spite of these large changes, several features of cortical organization showed little evidence of change, including cortical thickness, overall neuron size, and laminar organization. Estimates of total neuron number showed a trend level reduction of about 8%, due mainly to reduced cortical volume but unchanged neuron density. However, counts of calretinin (CR) and parvalbumin (PV) subtypes of GABAergic neurons showed a striking >30% reduction of neuron number. Similar ethanol effects were found in male and female mice, and in C57BL/6By and BALB/cJ mouse strains. Our findings indicate that the cortex has substantial capacity to develop normal cytoarchitectonic organization after early postnatal ethanol toxicity, but there is a selective and persistent reduction of GABA cells that may contribute to the lasting cognitive and behavioral deficits in FASD.

Keywords

fetal alcohol; interneuron; neocortex; gender difference; cortex thickness; stereology

Corresponding author: John F. Smiley, Ph.D., Nathan Kline Institute for Psychiatric Research, 140 Old Orangeburg Rd., Orangeburg, NY 10962, **Telephone:** +1 845 398 6601, **Fax:** +1 845 398 5531, smiley@nki.rfmh.org.

Introduction

Fetal alcohol spectrum disorders (FASD) are one of the most common causes of mental disabilities, and affect as many as 1% of children born in the United States (May et al., 2009). Along with cognitive deficits including memory, attention, and sensory perception, FASD is associated with reduced brain volume that persists into adulthood (Bakoyiannis et al., 2014; Norman, Crocker, Mattson, & Riley, 2009).

Animal models have been instrumental in providing insights into the brain areas and cellular processes that are affected by FASD. They have demonstrated that the effects of ethanol vary depending on the gestational timing of exposure. Treatment during the rodent early postnatal period, approximating the human third trimester, causes both widespread apoptotic cell death in the brain and long-lasting behavioral deficits (Ikonomidou et al., 2000; Sadrian, Wilson, & Saito, 2013; Wilson, Peterson, Basavaraj, & Saito, 2011; Wozniak et al., 2004). This is a period when neurogenesis is largely complete, and the brain is rapidly growing (Miller, 1988). Treatments early in this period, around the time of birth in rats, cause pronounced neurodegeneration in hypothalamic and ventral thalamic regions, compared to treatments around P3 that especially affect the dorsal thalamus and hippocampal regions, or treatments around P7 that especially affect cerebral cortex (Ikonomidou et al., 2000). Earlier treatments that model the first and second trimesters of human development also produce anatomical and behavioral changes, although they are somewhat distinct from the late gestational effects (Guerri, 1998; Sadrian et al., 2013). While these earlier ethanol treatments do not cause such widespread apoptosis, they have been shown to disrupt neurogenesis and cell migration (Cuzon, Yeh, Yanagawa, Obata, & Yeh, 2008).

Understanding the enduring effects of FASD on the brain is an area of ongoing research. In human adolescents and adults, FASD causes reduced volumes of gray matter and white matter throughout the forebrain. Gray matter volume reductions as large as 10% have been described across regions of the cerebral cortex, with even larger changes in subcortical structures, including hippocampus and striatum (Coles et al., 2011; Lebel et al., 2012; Nardelli, Lebel, Rasmussen, Andrew, & Beaulieu, 2011; Norman et al., 2009). Adult animals that were exposed to fetal alcohol typically have a similar profile of volume reductions (Coleman, Oguz, Lee, Styner, & Crews, 2012; Leigland, Ford, Lerch, & Kroenke, 2013). In some models, histological studies showed that these volume reductions corresponded to reduced neuron numbers (Berman & Hannigan, 2000; Ieraci & Herrera, 2007; Miller, 2006; Olney, 2004). More detailed examinations found evidence of altered dendritic length and spine density (Berman & Hannigan, 2000; Cui et al., 2010; Lawrence, Otero, & Kelly, 2012; Susick, Lowing, Provenzano, Hildebrandt, & Conti, 2014), and found evidence of disrupted organization of cortical sensory areas (Margret et al., 2006; Medina, Krahe, & Ramoa, 2005; Miller & Potempa, 1990). Additionally, in several cortical and subcortical brain regions there are findings of reduced GABAergic cell density, suggesting that inhibitory circuits in the cerebral cortex may be especially vulnerable to ethanol toxicity (Coleman et al., 2012; Sadrian, Lopez-Guzman, Wilson, & Saito, 2014; Sadrian et al., 2013). At present, it is unclear to what extent these changes are the direct result of cell loss induced by ethanol toxicity, or are secondary effects caused by compensatory brain plasticity that occurs in response to ethanol-induced damage. In particular, inhibition of

GABA function in early postnatal development is known to disrupt the normal development of cortical circuits (Le Magueresse & Monyer, 2013).

We recently demonstrated that mouse piriform cortex has reduced PV-immunolabeled GABA cells, along with increased neuron excitability, reduced paired-pulse inhibition, and enhanced oscillatory coherence, caused by ethanol treatment at both early and late gestational stages (Sadrian et al., 2013, 2014). The findings suggest that deficits of GABAergic inhibition may cause a characteristic profile of electrophysiological deficits. In the current study, we used a model of late gestational ethanol treatment (mouse P7) to determine whether a similar reduction in GABA cells is present throughout the neocortex, and we measured total neuron number to determine to what extent the neuron reduction was selective for GABAergic neurons. We also evaluated cortical thickness, surface area, and laminar organization, to evaluate the general features of adult cortical disruption caused by perinatal ethanol. Additionally, we included comparisons of C57BL/6By and BALB/cJ strains of mice, as these strains have well-established differences in alcohol preference and are commonly used as genetic animal models in alcohol-related research (Fish et al., 2010; Rodgers & McClearn, 1962; Vadasz, Baker, Joh, Lajtha, & Reis, 1982; Vadasz, Saito, et al., 2007).

Materials and methods

Subjects and ethanol exposure

Twenty-four mice were used, comparing 12 ethanol-treated to 12 saline-treated animals. The two treatment groups were matched to include equal numbers of C57BL/6By and BALB/cJ mice, with equal number of males and females from each strain. Mice were originally obtained from The Jackson Laboratory (Bar Harbor, Maine) in 1978, and maintained by brother × sister mating at the Nathan Kline Institute. Dams and their litters were housed individually in standard mouse cages, and maintained on *ad libitum* food and water. P7 pups were injected subcutaneously with saline or ethanol (2.5 g/kg) twice at 0 h and 2 h as described previously (Saito, Mao, Wang, Vadasz, & Saito, 2007) according to the methods originally described for C57BL/6 mice (Olney et al., 2002). This treatment induces a peak blood alcohol level of ~0.5 g/dL when the truncal blood is collected at 0.5, 1, 3, and 6 h following the second ethanol injection, as analyzed using Alcohol Reagent Set (Pointe Scientific, Canton, MI, USA) (Saito et al., 2007). This alcohol level is similar to those reported by others (Wozniak et al., 2004; Young & Olney, 2006). After injections, pups were returned to the litter, and weaning occurred at P25–30. All procedures were approved by the Nathan Kline Institute IACUC and were in accordance with NIH guidelines for the proper treatment of animals.

MRI data acquisition

After survival to 72–89 days of age, animals were anesthetized by intraperitoneal injection with 200 mg/kg ketamine and 10 mg/kg xylazine, and transcardially perfused with heparinized 4% paraformaldehyde in phosphate buffer, pH 7.2. The mouse heads were left in fixative overnight. The skin, lower jaw, ears, and cartilaginous nose tip were removed and the head placed in 50-mL tubes in 0.01% sodium azide in PBS for 3–7 days at 4 °C. The

head was then transferred to a 0.3% solution of MultiHance (gadobenate dimeglumine 529 mg/mL, Bracco Diagnostics Inc., Monroe Township, NJ, USA) and 0.01% sodium azide in PBS and rocked for 7 days at 4 °C. One day before the MRI scan, the head was placed in a 15-mL tube with the contrast reagent flombin (Sigma, catalog #317926). One day after scanning, the whole brain was removed and stored in phosphate-buffered saline with 0.03% sodium azide.

Images were acquired on a 7.0 Tesla Agilent (Santa Clara, CA) 40-cm bore system. The gradient coil insert had an internal diameter of 12 cm with a maximum gradient strength of 600 mT/m and minimum rise time of 200 μsec with customized second- and third-order shim coils. A Morris Instruments (Ontario, Canada) 1.5-cm inner diameter solenoid transmit coil was used for radiofrequency transmission and reception. The images used in this study were acquired with 150-μm^3 isotropic resolution and were taken from a data set of magnetic resonance diffusion measurements. For image analysis of 24 mouse brains, a mask was created automatically using the Automatic Registration Toolbox software (www.nitrc.org/projects/art). Individual brain extractions were manually corrected by using the ITK-snap (www.itk-snap.org) software and by consulting a mouse brain atlas (Paxinos & Franklin, 2004).

Histological processing and immunolabeling

Whole brain volumes, including cerebellum and brainstem, were measured by a fluid displacement method (Dorph-Petersen et al., 2005; Scherle, 1970). After cryoprotection by 2-day immersion in 20% buffered glycerol, brains were divided into two groups containing either 12 males or 12 females, and each group was embedded in a protein matrix for simultaneous sectioning and tissue processing (Smiley & Bleiwas, 2012). Coronally oriented brains were sectioned at 50-μm thickness. A series including every 6th consecutive section was mounted and dried on chrome-alum coated glass slides, and processed for Nissl staining with thionin before dehydration and coverslipping with Permount™.

For immunolabeling, neurons were visualized with mouse anti-PV diluted to 1:2,500 (Sigma, catalog #P3088) rabbit anti-CR diluted to 1:5,000 (Swant, catalog #7699/4) or mouse-anti-neuron specific protein (NeuN) diluted to 1:2,000 (Millipore, catalog #MAB377). For immunoperoxidase labeling with CR and PV antibodies, series of every 6th consecutive section were exposed to primary antibodies for 3 days in 1% normal serum, 0.03% Triton X-100, and phosphate buffer, pH 7.4, before processing with the streptavidin-biotin-peroxidase method and visualizing the label with diaminobenzidine. For immunofluorescence of PV and NeuN neurons, series of every 12th section were exposed to primary antibodies as above, followed by overnight exposure to Alexa Flour 488-conjugated goat anti-mouse or goat anti-rabbit secondary antibodies (Invitrogen, catalog #A11001 and #A11008). Sections processed for immunofluorescence were additionally labeled with 600 nM of the nuclear stain 4'6' diamino-2-phenylindole (DAPI; SIGMA, catalog #D9564). Immunofluorescence-labeled sections were coverslipped using Fluoro-Gel aqueous mounting medium (Electron Microscopy Sciences, catalog #17985-10).

Neocortex thickness, volume, and surface area

All microscopic imaging was done using ImageJ software to control a motorized Nikon E-600 microscope equipped with Ludl X, Y, and Z motors, a Heidenhain z-axis microcator, and a Foculus FO 442 digital camera (Net GMBH, Germany).

To simplify boundary identifications, we included neocortex that extended laterally to the edge of dysgranular limbic areas (i.e., piriform, insular, or ectorhinal cortex; Fig. 1). Medially, we used the border of the retrosplenial cortex in caudal sections where the hippocampus was visible. In sections that were more rostral, we used the midsagittal border with the corpus callosum. Rostral to the corpus callosum we included medial prefrontal cortex to the dorsopeduncular cortex, and additionally included orbitofrontal areas (Paxinos & Franklin, 2004).

Cortical thickness, surface area, and volume were sampled as previously described (Smiley et al., 2009). Using ImageJ software, photomontages (310 pixels per mm) were made of every Nissl-stained section, and tracings were made of the pial surface, layer IV/V border, and white matter border. Neocortex surface areas were derived from the summed length of the layer I tracings multiplied by the 0.3-mm section spacing, and neocortex volumes were the summed outlined areas multiplied by the section spacing. Thickness of the upper and lower layers was measured by software that periodically sampled the distance between each adjacent border. Total cortex thickness was the local sum of upper and lower cortex measurements. Thickness values were displayed as color flat maps, and thickness estimates were obtained by summing the numbers of rectangles of each color in outlined regions of interest (Fig. 1). For final estimates of cortical thickness, rostral sections more than one section in front of the anterior commissure were omitted, in order to avoid measuring tangentially cut rostral cortex. Additionally, midline cingulate cortex was omitted in order to avoid thickness distortions near the corpus callosum. Alternative measurements of cortical thickness that included rostral sections or cingulate cortex showed nearly identical groups comparisons (data not shown).

All of the above cortical shape measurements were done separately for the left and right hemispheres. However, as there was no evidence for hemispheric differences, or interactions between ethanol treatment and hemisphere, we combined data from the two hemispheres to simplify presentation of the results.

Neuron densities and numbers

Both 2-dimensional and 3-dimensional cell counting methods were used. For 2-dimensional measurements of immunoperoxidase-labeled PV and CR neurons, we developed a semi-automated thresholding method using ImageJ software. Gray-scale, tiled digital images were made of cerebral cortex, using a 10× objective (1.54 pixels/micron final magnification). To facilitate separation of cells from the local background, outline regions of cortex were divided into 65-micron wide squares. Each square was thresholded to a set value above the mode of its gray-scale density, and objects greater than about 6 μm in diameter were counted as cells. The locations of detected cells were displayed on the original image, so that invalid cell identifications could be manually edited. Measurements were taken from left

hemisphere neocortex, between the cingulate and retrosplenial areas medially, and the ectorhinal and insular cortex laterally, in 8–10 sections between bregma and 4 mm caudal to bregma (Fig. 2C).

3-dimensional stereological measurements to evaluate PV, CR, and NeuN cell densities and number were done using only the C57BL/6By mice. For this purpose, the optical disector method (Gundersen et al., 1988) was used on every 12th 50-μm section through the rostral-caudal extent of the left neocortex. A grid of optical disectors with 0.38-mm spacing was placed on each section, so that 264 ± 31 (mean ± S.D.) sites were sampled for each label from each animal. For each optical disector, the distance to pia and white matter was recorded, so that cell measurements could later be sorted by depth of cortex.

Immunofluorescent-labeled sections were used to count PV whole cells or NeuN nuclei. At each disector site, a z stack containing 6 images with 2-micron z-spacing was obtained near the upper tissue surface, using a 40× oil immersion with 1.3 numerical aperture. The camera shutter setting was automatically adjusted to maintain a narrow average gray-scale range for all captured z stacks. Counting boxes were drawn onto each z stack, with an upper guard zone consisting of two image slices, the counting box of three slices, and the bottom guard zone of one slice. The counting box X and Y dimensions were 200 μm and 144 μm, respectively, for PV, and 34 μm × 34 μm for NeuN. To definitively identify the borders of nuclei in NeuN cells, we additionally collected an identically focused stack from the DAPI staining at each disector site, and simultaneously viewed both labels while counting. To minimize tissue shrinkage, all fluorescent sections were stored at 4 °C and imaged within 1 week of coverslipping. Measurements of section thickness, taken in triplicate on each section, showed no significant z-axis shrinkage from the original 50 μm.

Stereological sampling of CR cells was done in immunoperoxidase-labeled tissue, where z-axis shrinkage facilitated efficient sampling of a greater number of cells per disector. Sampling methods were as used for PV cells, except using a 50× oil-immersion objective (1.3 numerical aperture), and correcting cell densities for z-axis shrinkage in each brain. Final section thickness tended to be thinner in ethanol-treated compared to saline-treated animals (13.6 ± 0.6 and 14.1 ± 0.3 μm, respectively, mean ± S.D., $p = 0.09$).

Estimates of measurement precision for cell densities and numbers (Dorph-Petersen et al., 2009) showed mean coefficients of error (CE) <0.1. Precision estimates for volumes of unilateral neocortex, using equations for the Cavalieri method (Gundersen, Jensen, Kiêu, & Nielsen, 1999), showed mean CE's <0.02.

Neuron size and immunolabeling density

Cell size was measured using the nucleator method (Gundersen, 1988). The average lengths of three isotropic lines, drawn from the approximate center of each cell to its border, were measured on each cell sampled by stereological cell counts. The CE's for all cell size measures (Dorph-Petersen, Pierri, Sun, Sampson, & Lewis, 2004) were <0.03.

Immunolabeling density was also sampled from each cell. Labeling density was evaluated as the absolute difference in gray-scale values between the mean density in a 5-micron

diameter circle at the center of the labeled cell and the modal gray scale value sampled in a circular band located at a radius of 20 to 28 microns from the cell center (Fig. 2G).

Statistical analysis

Data were subjected to univariate analysis of covariance (ANCOVA) using the General Linear Model as implemented in the IBM SPSS ver. 22 program. Besides the main analysis of ethanol effects, we included equal numbers of BALB/cJ and C57BL/6By mice, equally divided between males and females, in order to explore the effects of strain and sex on our anatomical measurements. For these reasons, ethanol effects were tested using univariate ANCOVA, including sex and strain as covariates. Additional comparison between sexes or between strains used ethanol treatment, and strain or sex, as covariates.

In 2-dimensional cell density measurements, PV cell density in one BALB/cJ animal was a statistical outlier, defined as greater than 2 standard deviations from the group mean. While this data point was omitted from the main analysis, an alternative analysis that included this datum is also described in the Results. A second BALB/cJ animal was excluded from the analyses of PV and CR immunohistochemistry because these labels failed, apparently due to poor fixation. In MRI whole-brain volume analysis, one ethanol-treated female C57BL/6By mouse was excluded from analysis because of poor image quality.

Results

Whole brain volume and body weight

Whole brain volumes measured by fluid displacement of isolated paraformaldehyde fixed brains were about 13% smaller in ethanol-treated compared to saline-treated mice ($p < 0.0001$, Table 1). A similar reduction (10%, $p < 0.001$) was obtained by imaging the brains with MRI before removal from the skull. Ethanol-treated mice also had about 8% reduced body weight ($p = 0.015$), suggesting that lower brain volume might be caused, at least in part, by decreased body size. However, partial correlation analysis did not show a close relationship between body weight and brain volume ($r = 0.155$, $p = 0.48$, using sex and ethanol treatment as covariates). Differences between mouse strains and sexes in body weight and other measures are discussed in a separate section below.

Neocortex volume, surface area, and thickness

The volume of the neocortex, measured in Nissl-stained sections, was about 12% smaller in ethanol-treated animals ($p < 0.001$). Measurements of surface area and thickness showed that reduced neocortical volume was mainly due to reduced surface area (9%, $p < 0.001$; Fig. 1). The small reduction of cortical thickness (3%) was not statistically significant ($p = 0.13$, Table 1).

Neuron densities and numbers

Cell counts were used to determine whether reduced cortical volumes corresponded to decreased neuron numbers (Fig. 2). Initial 2-dimensional counts of PV- and CR-immunoreactive GABA cells showed reduced densities of both cell types (PV, 19%, $p < 0.001$; CR 18%, $p < 0.001$). This analysis excluded one PV cell-density measurement that

was a statistical outlier (Fig. 3A). However, an alternative analysis that included this measurement showed a similar effect of ethanol (16% lower PV, $p < 0.02$). While there were also strain and sex differences in cell densities, similar ethanol effects were seen in both BALB/cJ and C57BL/6By mice, and in male and female animals (Fig. 3A–B and Table 1).

Three-dimensional cell counts using the optical disector method in the C57BL/6By animals confirmed the reductions of PV (29%, $p < 0.01$) and CR (26%, $p < 0.001$) neuron densities seen with 2-dimensional measurements (Fig. 3C). Estimates of total numbers that incorporate reduced cortex volume as well as neuron density indicated striking reductions of PV (34%, $p < 0.001$) and CR neurons (32%, $p < 0.001$; Table 1).

In contrast to the GABA cell types, 3-dimensional counts of total neurons, identified by NeuN immunolabeling, showed essentially unchanged neuron densities in ethanol-treated compared to saline-treated animals (2% lower in ethanol-treated animals, $p = 0.66$). Calculation of total neuron number showed a trend-level reduction of 8% ($p = 0.06$) in the ethanol-treated animals.

In order to explore the cortical distribution of these changes, the 3-dimensional neuron density measurements were separated by their rostral-caudal position across the cortex, or by their position in the depth of the cortex. These separations indicated that ethanol's effects on neuron densities were similar across regions and layers of the neocortex (Fig. 4).

Neuron immunolabeling density and size

A possible explanation of the finding of reduced neuron number is that neurons have reduced immunolabeling, for example, due to lower protein expression. However, measurement of labeling density in PV, CR, or NeuN cells counted with 3-dimensional methods did not reveal significant effects of ethanol treatment (Table 1).

Neuron size was additionally measured for all counted neurons. Group differences were not significant for any cell type (Table 1). However, separation of PV-positive cells by depth of cortex showed evidence of larger cells in approximately the upper 60% of the cortex, across rostral-caudal sections (Fig. 5). This size difference was statistically significant if only cells in the upper 60% of cortex were evaluated ($p < 0.05$).

Comparisons of mouse strains and sexes

Table 1 provides an overview of strain and sex comparisons for our anatomical measurements. While several measurements revealed strain and sex differences, these differences (expressed as ratios in Table 1) were generally comparable in the saline-treated and ethanol-treated groups, indicating that the two strains and two sexes were similarly affected by P7 ethanol treatment. One possible exception was cortex volume, which showed some evidence of greater ethanol-induced reduction in BALB/cJ compared to C57BL/6By mice. However, the ethanol × strain interaction effect was not statistically significant ($p = 0.16$, ANCOVA).

Several strain and sex differences were found. In both treated and untreated animals, body weight was about 20% greater in males than females ($p < 0.00001$, ANCOVA), and about

10% greater in C57BL/6By mice than BALB/cJ mice ($p < 0.01$). Similar strain and sex differences were not seen in whole-brain or neocortex volumes (p values >0.10).

Three-dimensional estimates of PV neuron number in C57BL/6By mice showed that females had as much as 36% greater PV neuron number than males ($p < 0.01$; Table 1), and 2-dimensional density measurements in C57BL/6By and BALB/cJ mice showed a similar gender effect ($p < 0.01$; Fig. 3, Table 1). This is consistent with a previous report of female>male difference in PV neuron number in rat prefrontal cortex (Wischhof, Irrsack, Osorio, & Koch, 2015). Additional gender comparisons from 3-dimensional measurements in C57BL/6By mice showed slightly larger CR neurons ($p < 0.01$), and greater total neuron numbers in males ($p < 0.05$). Strain comparisons, from 2-dimensional measurements, showed higher density of PV neurons ($p < 0.0001$, ANCOVA), and lower density of CR neurons ($p < 0.01$), in BALB/CJ compared to C57BL/6By mice (Fig. 3, Table 1).

Discussion

The ethanol treatment used in this study was previously shown to cause widespread cell death across the cerebral cortex within the first few days after treatment (Olney, 2004; Saito et al., 2007; Wilson et al., 2011). The goal of the present study was to determine to what extent the cell loss and cytoarchitectonic disruption caused by this treatment persist in the adult (>P70) neocortex. The findings showed several gross features of cortical organization to be largely unaltered, including cortical thickness and total neuronal density, size, and laminar organization. However, additional measurements demonstrated an overall reduction of about 12% in cortex volume, accompanied by about an 8% decrease of total neurons, and a comparatively severe reduction of approximately 30% of the GABA neuron subtypes that were sampled. At least within the resolution of our sampling paradigm, these changes were similar across the rostral-caudal extent of neocortex, and across all cortical layers.

Several mechanisms might explain the selective deficit of GABA neurons. One possibility is that GABA cells are selectively sensitive to ethanol toxicity at P7. At this time, both GABA and non-GABA cortical neurons are quite immature. The major wave of cortical neurogenesis is completed by several days before birth (Fairén, Cobas, & Fonseca, 1986; Rymar & Sadikot, 2007), and by about P3–7, most neurons have ended their migration to their final cortical positions (Miyoshi et al., 2010). The postnatal development of GABA cells to their mature form is an ongoing process that continues to adulthood (del Rio, de Lecea, Ferrer, & Soriano, 1994; Jiang, Huang, Morales, & Kirkwood, 2005). During the first postnatal week, there is an onset of rapid growth, including rapid increases of presynaptic terminals and inhibitory and excitatory postsynaptic currents (Le Magueresse & Monyer, 2013). It has been proposed that ethanol toxicity in P7 cortex is mediated in large part by inhibition of NMDA receptors and stimulation of GABA-A receptors (Ikonomidou et al., 2000). However, it has not been directly investigated whether P7 ethanol treatment selectively eliminates GABA cells, in part because most GABA-related cell markers are poorly expressed at this age (del Rio et al., 1994; Lema Tomé et al., 2008).

There is also evidence that neurogenesis after P7 ethanol treatment can shape the final adult composition of cortical neurons. For example, Coleman and colleagues (Coleman et al.,

2012) demonstrated increased neurogenesis in the mouse dentate gyrus in response to P7 ethanol treatment. In the cerebral cortex, application of hypoxia to mice at P3–P10 caused increased neurogenesis, with new neurons at least partially originating from glial fibrillary acid protein (GFAP)-expressing cells in the cortical plate (Bi et al., 2011; Fagel et al., 2006). The authors suggested that this might account for the observation that the nearly 30% neuron loss seen at P11 was no longer detectable at day P18. Notably, they also found that this normalization of total neuron number was not accompanied by a corresponding recovery of PV-and CR-GABAergic cells, which continued to show a 30% reduction in adult animals (Fagel et al., 2009). If similar mechanisms occur in our ethanol-treated mice, these findings suggest that the deficit in GABA number may reflect compensatory neurogenesis that occurs mainly in non-GABAergic neurons of the cortex.

Yet another possible explanation for selectively reduced GABA cells is that they are still present in the cortex, but have suppressed expression of GABA-related proteins such as PV and CR. This scenario was supported in the P3–P10 hypoxia-treated mouse model, where a 30% reduction was found in immunolabeled GABA neurons, but was not seen using GABA cells identified by GAD67-enhanced green fluorescence protein (EGF) in transgenic mice (Komitova et al., 2013). The authors additionally showed that the density of GABA cell immunolabeling could be upregulated in these mice by exposure to an enriched environment. However, it remains to be demonstrated whether a similar explanation is relevant to our ethanol reduction of GABA cells. Notably, Komitova and colleagues (2013) showed that the hypoxia-induced reduction of GABA cell number was accompanied by reduced immunolabeling density in PV and somatostatin cells, and by reduced cell diameter in PV cells. In contrast, we did not find reduced PV- or CR-immunolabeling density, and found some evidence for increased diameter of PV cells.

Additionally, there is some neurogenesis of cortical GABAergic interneurons that continues postnatally, originating from stem cells in the subventricular zone and white matter beneath the cingulate cortex (Inta et al., 2008; Le Magueresse et al., 2011; Riccio et al., 2012). These stem cells produce GABA cells mainly in the first postnatal week, and less in subsequent weeks. It is possible that ethanol toxicity at P7 inhibits this source of cortical GABA cells. However, descriptions of these cells indicated that they are a comparatively minor fraction of the total GABA cell population, that they include CR but not PV cells, and that they migrate mainly into cortical layers V and VI. Therefore, if ethanol inhibits this late wave of GABA cell neurogenesis, it probably would account for only a fraction of the GABA cell reduction we observed in CR and PV cells throughout the depth of cortex.

It remains to be demonstrated whether other types of cortical GABA cells are similarly reduced by P7 ethanol treatment. The CR and PV cells that we counted comprise about 1/3 of the total GABA population, and represent non-overlapping and distinct subtypes of GABA cells (Miyoshi et al., 2010). Whereas PV cells are often fast-spiking feed-forward cells, CR cells are typically non-fast spiking bipolar or double-bouquet type cells (Kawaguchi & Kondo, 2002). Whereas rodent PV cells originate from neurogenesis in the medial ganglionic eminence, CR cells originate in the caudal ganglionic eminence (Miyoshi et al., 2010; Rymar & Sadikot, 2007). Our results extend previous findings that immunolabeled PV cells are reduced in animal models of late gestational ethanol toxicity, in

frontal cortex (Coleman et al., 2012), cingulate cortex (Moore, Ruygrok, Walker, & Heaton, 1997), piriform cortex and hippocampus (Sadrian et al., 2014), the medial septal area (Mitchell, Paiva, & Heaton, 2000), and striatum (De Giorgio, Comparini, Intra, & Granato, 2012). Our findings seem to contradict a finding of increased CR and unchanged PV cell density in rat cortex, after ethanol treatment at days P2–P6 (Granato, 2006).

In early gestation models of alcohol toxicity, reduced GABA cell density has also been observed, but its features are somewhat different. For example, treatment of monkeys in early gestation or throughout pregnancy caused decreased GABA cell density, but it was not proportionally greater than the decrease of total neuron density (Miller, 2006). In mouse piriform cortex, ethanol causes reduced PV cell density at both late and early gestational periods, but in the hippocampus it reduces PV cell density with late treatment, but increases it with early treatment (Sadrian et al., 2014).

It might be expected that widespread death in the early postnatal cerebral cortex would cause the adult cortex to be thinner, or alternatively to have decreased total neuron density. However, our findings showed that the reductions in cortical volume (12%) and total neuron number (8%) were accompanied mainly by about 9% lower surface area, with very minor net reductions in neuron density (2%) and cortical thickness (3%) that were not significant in our sample. These findings suggest that the immature cortex has significant capacity to recover from the cell death caused by P7 ethanol, either by upregulating neurogenesis as discussed above, or perhaps additionally by reorganizing the remaining neurons into approximately normal cortical organization in the adult animal. Previous mapping of cortical thickness also revealed evidence of dynamic response to ethanol treatment. In rats, ethanol applied throughout gestation caused slightly thinner cortex at P11, but cortical thickness was nearly normal by P60, even though reduced volume and surface area persisted (Leigland et al., 2013). In adolescent and adult FASD subjects, cerebral cortex was found to be thicker than controls, perhaps reflecting compensatory development after ethanol-induced damage (Fernández-Jaén et al., 2011; Sowell et al., 2008; Yang et al., 2012). However, there is also a finding of thinner cortex in FASD subjects (Zhou et al., 2011).

Besides decreased GABA cell labeling and total neuron number, our measurements of total neuron density, laminar organization, and cortical thickness did not show obvious changes in ethanol-treated animals. Additional analyses of specific areas and cell types might reveal anatomical changes beneath the resolution of our measurements. For example, disrupted columnar organization was found in somatosensory and visual cortex after prolonged gestational ethanol exposure (Margret et al., 2006; Medina & Ramoa, 2005; Miller & Potempa, 1990). Another study showed changes in pyramidal cell dendritic length after early postnatal ethanol (Granato & De Giorgio, 2014).

We additionally tested whether C57BL/6By and BALB/cJ mouse strains have different long-term responses to early ethanol treatment. There is strong evidence that alcohol consumption phenotypes are heritable, and these strains are commonly used as genetic animal models of alcohol consumption and alcoholism (Rodgers & McClearn, 1962; Vadász, Fleischer, LaFrancois, & Mao, 1996). We and others have shown that C57BL/6J mice have alcohol-preferring behavior, in contrast to alcohol-avoiding behavior in BALB/cJ

mice (Rodgers & McClearn, 1962; Vadasz, Saito, et al., 2007). In the present experiments, we did not observe differences between these strains in the long-term cellular deficits caused by P7 alcohol toxicity. However, our cell density measurements showed strain differences in the normal complement of cortical GABA cells in these strains, with proportionally fewer PV neurons and more CR neurons in C57BL/6By mice. These differences may be relevant to the alcohol-related behaviors that distinguish these strains, similar, for example, to previously described differences in dopamine cell number (Vadasz, Smiley, et al., 2007).

In summary, our findings in adult animals showed a modest trend-level reduction of total cortical neuron number, accompanied by a proportionally much greater reduction in the number of immunolabeled PV and CR neurons. It remains to be determined whether the reduction of GABA cells represents actual cell loss, or alternatively represents reduction of GABA-related proteins in these cells. In either case, our findings suggest that GABAergic neurotransmission is altered throughout the cerebral cortex. GABA is known to be a critical modulator of brain development, and its reduction during critical periods alters normal development of cortical circuits (Le Magueresse & Monyer, 2013). In the adult, reduced GABA neurotransmission is thought to contribute to hyperexcitability and disrupted cortical oscillations that have been noted in various developmental disorders (Sadrian et al., 2013). Our findings that several gross features of cortex, such as thickness and laminar organization, are largely normal in the adult animal, is consistent with previous observations that the cortex has substantial capacity to overcome perinatal disruption.

Acknowledgments

This research was supported by NIAAA grant AA023181 and NIMH grant MH086385.

References

Bakoyiannis I, Gkioka E, Pergialiotis V, Mastroleon I, Prodromidou A, Vlachos GD, et al. Fetal alcohol spectrum disorders and cognitive functions of young children. Reviews in the Neurosciences. 2014; 25:631–639. [PubMed: 24978898]

Berman RF, Hannigan JH. Effects of prenatal alcohol exposure on the hippocampus: spatial behavior, electrophysiology, and neuroanatomy. Hippocampus. 2000; 10:94–110. [PubMed: 10706221]

Bi B, Salmaso N, Komitova M, Simonini MV, Silbereis J, Cheng E, et al. Cortical glial fibrillary acidic protein-positive cells generate neurons after perinatal hypoxic injury. The Journal of Neuroscience. 2011; 31:9205–9221. [PubMed: 21697371]

Coleman LG Jr, Oguz I, Lee J, Styner M, Crews FT. Postnatal day 7 ethanol treatment causes persistent reductions in adult mouse brain volume and cortical neurons with sex specific effects on neurogenesis. Alcohol. 2012; 46:603–612. [PubMed: 22572057]

Coles CD, Goldstein FC, Lynch ME, Chen X, Kable JA, Johnson KC, et al. Memory and brain volume in adults prenatally exposed to alcohol. Brain and Cognition. 2011; 75:67–77. [PubMed: 21067853]

Cui ZJ, Zhao KB, Zhao HJ, Yu DM, Niu YL, Zhang JS, et al. Prenatal alcohol exposure induces long-term changes in dendritic spines and synapses in the mouse visual cortex. Alcohol and Alcoholism. 2010; 45:312–319. [PubMed: 20543181]

Cuzon VC, Yeh PW, Yanagawa Y, Obata K, Yeh HH. Ethanol consumption during early pregnancy alters the disposition of tangentially migrating GABAergic interneurons in the fetal cortex. The Journal of Neuroscience. 2008; 28:1854–1864. [PubMed: 18287502]

De Giorgio A, Comparini SE, Intra FS, Granato A. Long-term alterations of striatal parvalbumin interneurons in a rat model of early exposure to alcohol. Journal of Neurodevelopmental Disorders. 2012; 4:18. [PubMed: 22958715]

del Rio JA, de Lecea L, Ferrer I, Soriano E. The development of parvalbumin-immunoreactivity in the neocortex of the mouse. Brain Research. Developmental Brain Research. 1994; 81:247–259. [PubMed: 7813046]

Dorph-Petersen KA, Caric D, Saghafi R, Zhang W, Sampson AR, Lewis DA. Volume and neuron number of the lateral geniculate nucleus in schizophrenia and mood disorders. Acta Neuropathologica. 2009; 117:369–384. [PubMed: 18642008]

Dorph-Petersen KA, Pierri JN, Perel JM, Sun Z, Sampson AR, Lewis DA. The influence of chronic exposure to antipsychotic medications on brain size before and after tissue fixation: a comparison of haloperidol and olanzapine in macaque monkeys. Neuropsychopharmacology. 2005; 30:1649–1661. [PubMed: 15756305]

Dorph-Petersen KA, Pierri JN, Sun Z, Sampson AR, Lewis DA. Stereological analysis of the mediodorsal thalamic nucleus in schizophrenia: volume, neuron number, and cell types. The Journal of Comparative Neurology. 2004; 472:449–462. [PubMed: 15065119]

Fagel DM, Ganat Y, Cheng E, Silbereis J, Ohkubo Y, Ment LR, et al. Fgfr1 is required for cortical regeneration and repair after perinatal hypoxia. The Journal of Neuroscience. 2009; 29:1202–1211. [PubMed: 19176828]

Fagel DM, Ganat Y, Silbereis J, Ebbitt T, Stewart W, Zhang H, et al. Cortical neurogenesis enhanced by chronic perinatal hypoxia. Experimental Neurology. 2006; 199:77–91. [PubMed: 15916762]

Fairén A, Cobas A, Fonseca M. Times of generation of glutamic acid decarboxylase immunoreactive neurons in mouse somatosensory cortex. The Journal of Comparative Neurology. 1986; 251:67–83. [PubMed: 3760259]

Fernández-Jaén A, Fernández-Mayoralas DM, Quiñones Tapia D, Calleja-Pérez B, García- Segura JM, Arribas SL, et al. Cortical thickness in fetal alcohol syndrome and attention deficit disorder. Pediatric Neurology. 2011; 45:387–391. [PubMed: 22115001]

Fish EW, Riday TT, McGuigan MM, Faccidomo S, Hodge CW, Malanga CJ. Alcohol, cocaine, and brain stimulation-reward in C57Bl6/J and DBA2/J mice. Alcoholism: Clinical and Experimental Research. 2010; 34:81–89.

Granato A. Altered organization of cortical interneurons in rats exposed to ethanol during neonatal life. Brain Research. 2006; 1069:23–30. [PubMed: 16386714]

Granato A, De Giorgio A. Alterations of neocortical pyramidal neurons: turning points in the genesis of mental retardation. Frontiers in Pediatrics. 2014; 2:86. [PubMed: 25157343]

Guerri C. Neuroanatomical and neurophysiological mechanisms involved in central nervous system dysfunctions induced by prenatal alcohol exposure. Alcoholism: Clinical and Experimental Research. 1998; 22:304–312.

Gundersen HJ. The nucleator. Journal of Microscopy. 1988; 151:3–21. [PubMed: 3193456]

Gundersen HJ, Jensen EB, Kiêu K, Nielsen J. The efficiency of systematic sampling in stereology--reconsidered. Journal of Microscopy. 1999; 193:199–211. [PubMed: 10348656]

Gundersen HJ, Bagger P, Bendtsen TF, Evans SM, Korbo L, Marcussen N, et al. The new stereological tools: disector, fractionator, nucleator and point sampled intercepts and their use in pathological research and diagnosis. Acta Pathologica, Microbiologica, et Immunologica Scandinavica. 1988; 96:857–881.

Ieraci A, Herrera DG. Single alcohol exposure in early life damages hippocampal stem/progenitor cells and reduces adult neurogenesis. Neurobiology of Disease. 2007; 26:597–605. [PubMed: 17490887]

Ikonomidou C, Bittigau P, Ishimaru MJ, Wozniak DF, Koch C, Genz K, et al. Ethanol-induced apoptotic neurodegeneration and fetal alcohol syndrome. Science. 2000; 287:1056–1060. [PubMed: 10669420]

Inta D, Alfonso J, von Engelhardt J, Kreuzberg MM, Meyer AH, van Hooft JA, et al. Neurogenesis and widespread forebrain migration of distinct GABAergic neurons from the postnatal subventricular zone. Proceedings of the National Academy of the United States of America. 2008; 105:20994–20999.

Jiang B, Huang ZJ, Morales B, Kirkwood A. Maturation of GABAergic transmission and the timing of plasticity in visual cortex. Brain Research. Brain Research Reviews. 2005; 50:126–133. [PubMed: 16024085]

Kawaguchi Y, Kondo S. Parvalbumin, somatostatin and cholecystokinin as chemical markers for specific GABAergic interneuron types in the rat frontal cortex. Journal of Neurocytology. 2002; 31:277–287. [PubMed: 12815247]

Komitova M, Xenos D, Salmaso N, Tran KM, Brand T, Schwartz ML, et al. Hypoxia-induced developmental delays of inhibitory interneurons are reversed by environmental enrichment in the postnatal mouse forebrain. The Journal of Neuroscience. 2013; 33:13375–13387. [PubMed: 23946395]

Lawrence RC, Otero NK, Kelly SJ. Selective effects of perinatal ethanol exposure in medial prefrontal cortex and nucleus accumbens. Neurotoxicology and Teratology. 2012; 34:128–135. [PubMed: 21871563]

Le Magueresse C, Alfonso J, Khodosevich K, Arroyo Martin AA, Bark C, Monyer H. "Small axonless neurons": postnatally generated neocortical interneurons with delayed functional maturation. The Journal of Neuroscience. 2011; 31:16731–16747. [PubMed: 22090500]

Le Magueresse C, Monyer H. GABAergic interneurons shape the functional maturation of the cortex. Neuron. 2013; 77:388–405. [PubMed: 23395369]

Lebel C, Mattson SN, Riley EP, Jones KL, Adnams CM, May PA, et al. A longitudinal study of the long-term consequences of drinking during pregnancy: heavy in utero alcohol exposure disrupts the normal processes of brain development. The Journal of Neuroscience. 2012; 32:15243–15251. [PubMed: 23115162]

Leigland LA, Ford MM, Lerch JP, Kroenke CD. The influence of fetal ethanol exposure on subsequent development of the cerebral cortex as revealed by magnetic resonance imaging. Alcoholism: Clinical and Experimental Research. 2013; 37:924–932.

Lema Tomé CM, Miller R, Bauer C, Smith C, Blackstone K, Leigh A, et al. Decline in age-dependent, MK801-induced injury coincides with developmental switch in parvalbumin expression: somatosensory and motor cortex. Developmental Psychobiology. 2008; 50:665–679. [PubMed: 18688810]

Margret CP, Li CX, Chappell TD, Elberger AJ, Matta SG, Waters RS. Prenatal alcohol exposure delays the development of the cortical barrel field in neonatal rats. Experimental Brain Research. 2006; 172:1–13. [PubMed: 16506013]

May PA, Gossage JP, Kalberg WO, Robinson LK, Buckley D, Manning M, et al. Prevalence and epidemiologic characteristics of FASD from various research methods with an emphasis on recent in-school studies. Developmental Disabilities Research Reviews. 2009; 15:176–192. [PubMed: 19731384]

Medina AE, Krahe TE, Ramoa AS. Early alcohol exposure induces persistent alteration of cortical columnar organization and reduced orientation selectivity in the visual cortex. Journal of Neurophysiology. 2005; 93:1317–1325. [PubMed: 15483067]

Medina AE, Ramoa AS. Early alcohol exposure impairs ocular dominance plasticity throughout the critical period. Brain Research. Developmental Brain Research. 2005; 157:107–111. [PubMed: 15939092]

Miller MW. Effect of prenatal exposure to ethanol on the development of cerebral cortex: I. Neuronal generation. Alcoholism: Clinical and Experimental Research. 1988; 12:440–449.

Miller MW. Effect of prenatal exposure to ethanol on glutamate and GABA immunoreactivity in macaque somatosensory and motor cortices: critical timing of exposure. Neuroscience. 2006; 138:97–107. [PubMed: 16427209]

Miller MW, Potempa G. Numbers of neurons and glia in mature rat somatosensory cortex: effects of prenatal exposure to ethanol. The Journal of Comparative Neurology. 1990; 293:92–102. [PubMed: 2312794]

Mitchell JJ, Paiva M, Heaton MB. Effect of neonatal ethanol exposure on parvalbumin-expressing GABAergic neurons of the rat medial septum and cingulate cortex. Alcohol. 2000; 21:49–57. [PubMed: 10946157]

Miyoshi G, Hjerling-Leffler J, Karayannis T, Sousa VH, Butt SJ, Battiste J, et al. Genetic fate mapping reveals that the caudal ganglionic eminence produces a large and diverse population of superficial cortical interneurons. The Journal of Neuroscience. 2010; 30:1582–1594. [PubMed: 20130169]

Moore DB, Ruygrok AC, Walker DW, Heaton MB. Effects of prenatal ethanol exposure on parvalbumin-expressing GABAergic neurons in the adult rat medial septum. Alcoholism: Clinical and Experimental Research. 1997; 21:849–856.

Nardelli A, Lebel C, Rasmussen C, Andrew G, Beaulieu C. Extensive deep gray matter volume reductions in children and adolescents with fetal alcohol spectrum disorders. Alcoholism: Clinical and Experimental Research. 2011; 35:1404–1417.

Norman AL, Crocker N, Mattson SN, Riley EP. Neuroimaging and fetal alcohol spectrum disorders. Developmental Disabilities Research Reviews. 2009; 15:209–217. [PubMed: 19731391]

Olney JW. Fetal alcohol syndrome at the cellular level. Addiction Biology. 2004; 9:137–149. discussion 151. [PubMed: 15223539]

Olney JW, Tenkova T, Dikranian K, Muglia LJ, Jermakowicz WJ, D'Sa C, et al. Ethanol-induced caspase-3 activation in the in vivo developing mouse brain. Neurobiology of Disease. 2002; 9:205–219. [PubMed: 11895372]

Paxinos, G.; Franklin, KBJ. The Mouse Brain in Sterotaxic Coordinates. London, UK: Academic Press; 2004.

Riccio O, Murthy S, Szabo G, Vutskits L, Kiss JZ, Vitalis T, et al. New pool of cortical interneuron precursors in the early postnatal dorsal white matter. Cerebral Cortex. 2012; 22:86–98. [PubMed: 21616983]

Rodgers DA, McClearn GE. Mouse strain differences in preference for various concentrations of alcohol. Quarterly Journal of Studies on Alcohol. 1962; 23:26–33. [PubMed: 14493106]

Rymar VV, Sadikot AF. Laminar fate of cortical GABAergic interneurons is dependent on both birthdate and phenotype. The Journal of Comparative Neurology. 2007; 501:369–380. [PubMed: 17245711]

Sadrian B, Lopez-Guzman M, Wilson DA, Saito M. Distinct neurobehavioral dysfunction based on the timing of developmental binge-like alcohol exposure. Neuroscience. 2014; 280:204–219. [PubMed: 25241068]

Sadrian B, Wilson DA, Saito M. Long-lasting neural circuit dysfunction following developmental ethanol exposure. Brain Sciences. 2013; 3:704–727. [PubMed: 24027632]

Saito M, Mao RF, Wang R, Vadasz C, Saito M. Effects of gangliosides on ethanol-induced neurodegeneration in the developing mouse brain. Alcoholism: Clinical and Experimental Research. 2007; 31:665–674.

Scherle W. A simple method for volumetry of organs in quantitative stereology. Mikroskopie. 1970; 26:57–60. [PubMed: 5530651]

Smiley JF, Bleiwas C. Embedding matrix for simultaneous processing of multiple histological samples. Journal of Neuroscience Methods. 2012; 209:195–198. [PubMed: 22710286]

Smiley JF, Rosoklija G, Mancevski B, Mann JJ, Dwork AJ, Javitt DC. Altered volume and hemispheric asymmetry of the superficial cortical layers in the schizophrenia planum temporale. European Journal of Neuroscience. 2009; 30:449–463. [PubMed: 19656176]

Sowell ER, Mattson SN, Kan E, Thompson PM, Riley EP, Toga AW. Abnormal cortical thickness and brain-behavior correlation patterns in individuals with heavy prenatal alcohol exposure. Cerebral Cortex. 2008; 18:136–144. [PubMed: 17443018]

Susick LL, Lowing JL, Provenzano AM, Hildebrandt CC, Conti AC. Postnatal ethanol exposure simplifies the dendritic morphology of medium spiny neurons independently of adenylyl cyclase 1 and 8 activity in mice. Alcoholism: Clinical and Experimental Research. 2014; 38:1339–1346.

Vadasz C, Baker H, Joh TH, Lajtha A, Reis DJ. The inheritance and genetic correlation of tyrosine hydroxylase activities in the substantia nigra and corpus striatum in the C × B recombinant inbred mouse strains. Brain Research. 1982; 234:1–9. [PubMed: 6120745]

Vadász C, Fleischer A, LaFrancois J, Mao RF. Self-administration of ethanol: towards the location of predisposing polygenes in quasi-congenic animal models. Alcohol. 1996; 13:617–620. [PubMed: 8949958]

Vadasz C, Saito M, Gyetvai BM, Oros M, Szakall I, Kovacs KM, et al. Mapping of QTLs for oral alcohol self-administration in B6.C and B6.I quasi-congenic RQI strains. Neurochemical Research. 2007; 32:1099–1112. [PubMed: 17273929]

Vadasz C, Smiley JF, Figarsky K, Saito M, Toth R, Gyetvai BM, et al. Mesencephalic dopamine neuron number and tyrosine hydroxylase content: Genetic control and candidate genes. Neuroscience. 2007; 149:561–572. [PubMed: 17920205]

Wilson DA, Peterson J, Basavaraj BS, Saito M. Local and regional network function in behaviorally relevant cortical circuits of adult mice following postnatal alcohol exposure. Alcoholism: Clinical and Experimental Research. 2011; 35:1974–1984.

Wischhof L, Irrsack E, Osorio C, Koch M. Prenatal LPS-exposure--a neurodevelopmental rat model of schizophrenia--differentially affects cognitive functions, myelination and parvalbumin expression in male and female offspring. Progress in Neuro-psychopharmacology & Biological Psychiatry. 2015; 57:17–30. [PubMed: 25455585]

Wozniak DF, Hartman RE, Boyle MP, Vogt SK, Brooks AR, Tenkova T, et al. Apoptotic neurodegeneration induced by ethanol in neonatal mice is associated with profound learning/memory deficits in juveniles followed by progressive functional recovery in adults. Neurobiology of Disease. 2004; 17:403–414. [PubMed: 15571976]

Yang Y, Roussotte F, Kan E, Sulik KK, Mattson SN, Riley EP, et al. Abnormal cortical thickness alterations in fetal alcohol spectrum disorders and their relationships with facial dysmorphology. Cerebral Cortex. 2012; 22:1170–1179. [PubMed: 21799209]

Young C, Olney JW. Neuroapoptosis in the infant mouse brain triggered by a transient small increase in blood alcohol concentration. Neurobiology of Disease. 2006; 22:548–554. [PubMed: 16459096]

Zhou D, Lebel C, Lepage C, Rasmussen C, Evans A, Wyper K, et al. Developmental cortical thinning in fetal alcohol spectrum disorders. Neuroimage. 2011; 58:16–25. [PubMed: 21704711]

Highlights

- A mouse model of fetal alcohol disorders was evaluated for anatomical changes in cerebral cortex.
- Cortex surface area was reduced, but its thickness and laminar organization were largely normal.
- While total neuron number was about 8% lower, GABA neurons were > 30% reduced.
- The selective reduction of GABA neurons was present throughout the cerebral cortex.
- Reduced GABA may contribute to cognitive deficits in fetal alcohol disorders.

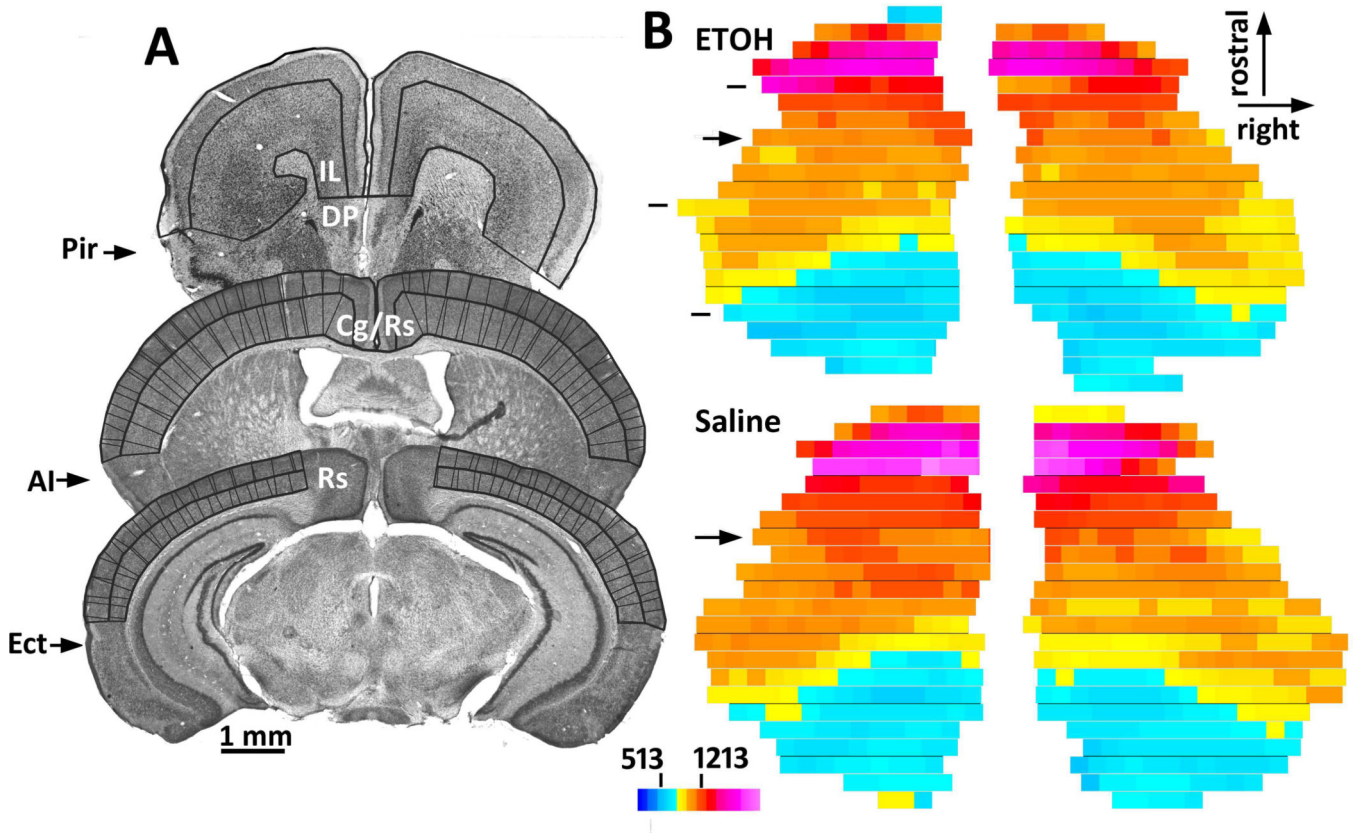

Figure 1.

Volume, surface area, and thickness were measured in the region of neocortex. **A**. Nissl-stained sections are shown to illustrate the region of neocortex that was sampled for anatomical measurements. Thick lines show the tracings of the pial surface, layer IV/V border, and white matter border that were used for volume and surface area measurements. For these measurements, midline infralimbic and cingulate areas were included, but midline retrosplenial cortex was excluded caudal to the most rostral section through the hippocampus. Laterally, cortex was included to the border of agranular areas. Cortex thickness measurements (thin lines) excluded sections rostral to the section in front of the anterior commissure; additionally excluded was the midline cingulate cortex. **B**. Cortical thickness measurements from consecutive Nissl sections were displayed as colored flat maps. In these examples, all sections to the frontal pole are displayed for the purpose of illustration. However, sections more than one section rostral to the anterior commissure (arrows) were omitted from the main analysis. The difference between these two example plots is approximately representative of the larger groups: this ethanol-treated animal had about 4% thinner cortex and about 12% less surface area compared to this saline-treated animal. The dashed lines at the left of the upper plot show the locations of the three sections in A. The scale bars show the limits of cortical thickness (513 and 1213 microns) that were included in the analysis of these two brains. Abbreviations: AI, agranular insular cortex; Cg, cingulated cortex; DP, dorsopeduncular cortex; Ect, ectorhinal cortex; IL, infralimbic cortex; Pir, piriform cortex; Rs, retrosplenial cortex.

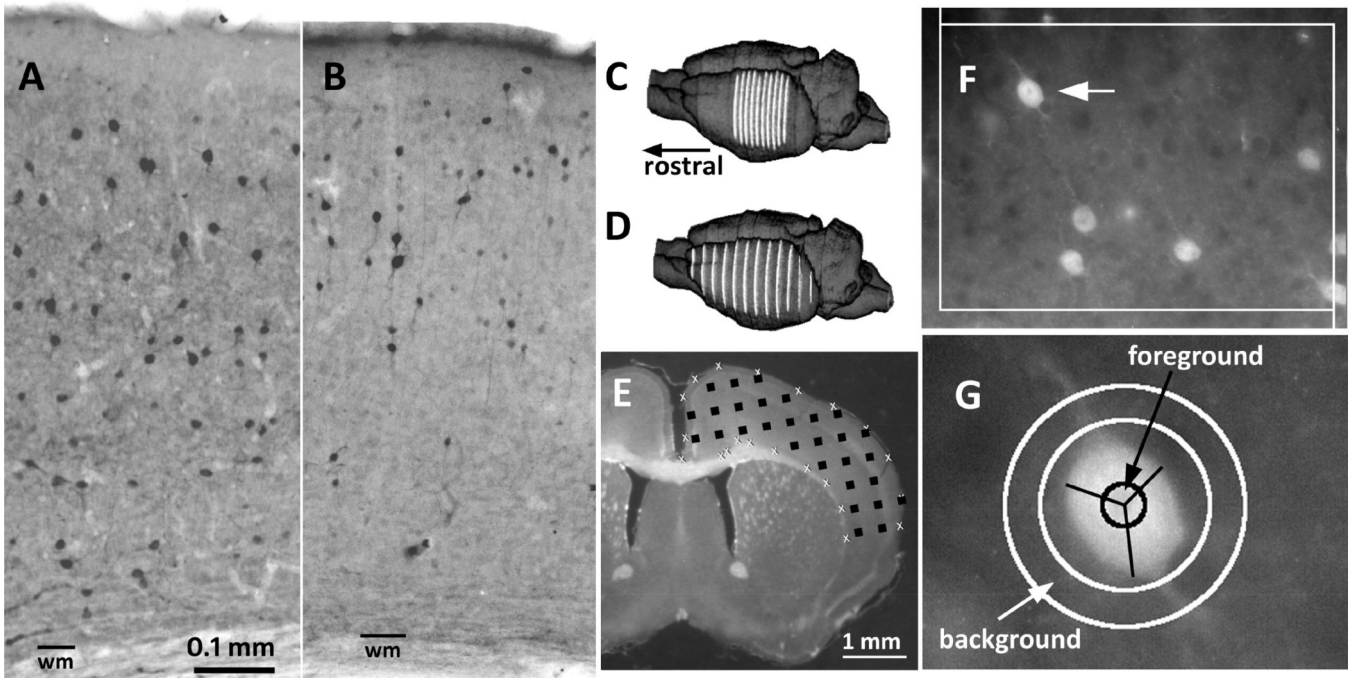

Figure 2.

Examples are shown of the methods used to measure cell density, size, and cell labeling density. **A–B**. For 2-dimensional cell counting, peroxidase-immunolabeled PV cells (A) or CR cells (B) were counted across the depth of cortex. **C**. The location of cortex used for 2-dimensional cell density measurements is shown on a reconstruction of one brain, made from block face images taken during sectioning. From 8 to 10 sections (white lines) were sampled between bregma and 4 mm caudal to bregma. **D**. For 3-dimensional neuron counts, every 12th 50-μm thick section through neocortex was sampled. **E**. Neurons in neocortex were sampled using the optical disector method, with an evenly spaced grid of sampling sites (black squares). **F**. An example is shown of the optical-disector counting box used to sample PV neurons. Box size is 200 μm wide. The arrow shows the location of the counted PV neuron displayed in G below. **G**. Cell-labeling density and size was evaluated for neurons counted in the optical disectors. Labeling density for each cell was the difference between mean gray-scale density at the cell center (black circle) and the modal-gray density in a band located 20–28 microns from the cell center. Cell size was evaluated by measuring three isotropic lines (black lines) from the cell center to its periphery. Abbreviation: wm, white matter.

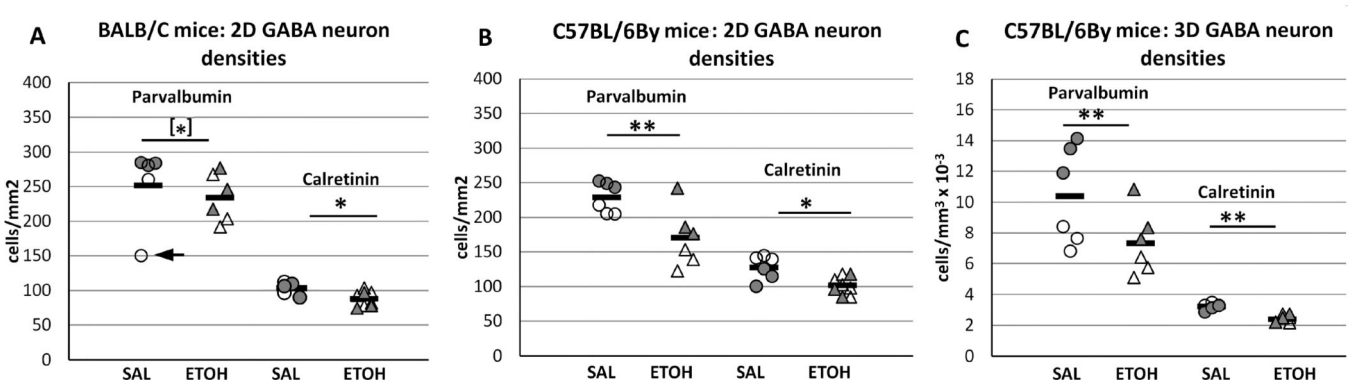

Figure 3.

Counts of parvalbumin (PV) and calretinin (CR) neurons in neocortex were done by 2-dimensional (2D) and 3-dimensional (3D) methods. Filled symbols show counts from female animals. **A**. In the initial 2-dimensional cell counts in BALB/cJ sample, one saline-treated animal was excluded due to poor labeling. A second saline-treated animal had PV neuron density that was a statistical outlier (arrow). **B**. 2-D measurements in C57BL/6By animals showed ethanol effects similar to that of BALB/cJ animals. ANCOVA analysis of all 2-dimensional measurements showed a highly significant effect of ethanol in both CR and PV neurons, and a female>male gender difference in PV neuron density. Additionally, there was evidence of strain differences, with higher PV neuron density and lower CR neuron density in BALB/cJ mice. **C**. 3-D measurements of PV and CR neuron density in the C57BL/6By animals confirmed the ethanol and gender differences seen with 2-D measurements. *$p < 0.05$, **$p < 0.01$, [*]$p < 0.05$ if outlier is omitted.

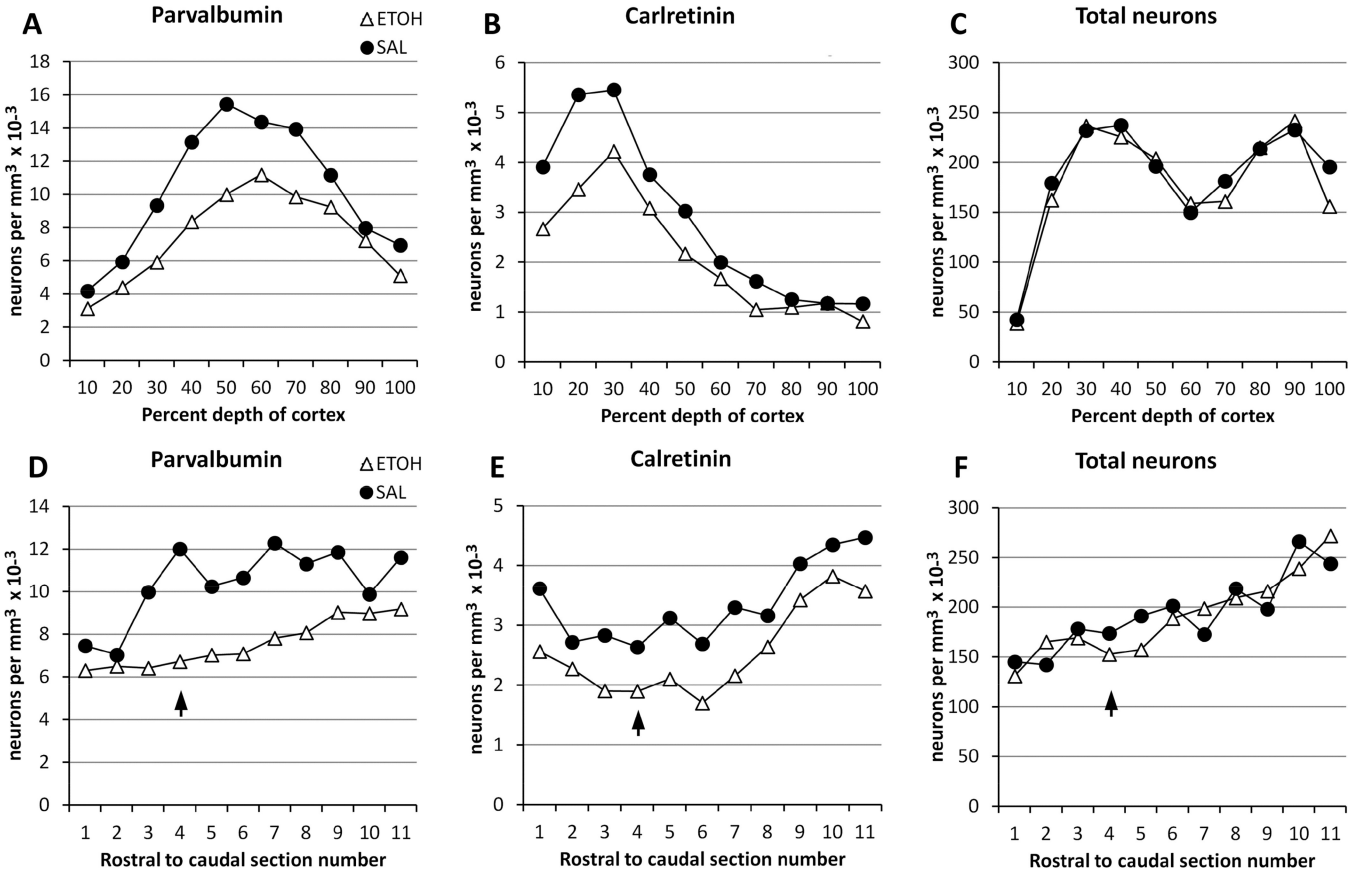

Figure 4.

Three-dimensional cell density measurements in C57BL/6By mice were further separated by percent depth of cortex, or by rostral-caudal section. It should be noted that these histograms give a qualitative overview of local differences: each data point includes only about 30 counted cells, and individual points lack statistical power to show definitive changes. **A–C**. The lower density of PV and CR cells in ethanol-treated animals was similar in all cortical layers. Total neurons, identified by NeuN-cell immunolabeling, showed similar laminar distributions in the two groups. **D–F**. The lower density of PV and CR cells in ethanol-treated animals was similar across rostral-caudal sections. NeuN-cell densities showed very similar rostral-caudal distribution in the two groups. In graphs of rostral-caudal sections, a few brains had more than 11 sections, and the final sections with small cell numbers were omitted. Closed circles = salinetreated, and open triangles = ethanol-treated animals. Arrows = the approximate location of the rostral edge of the anterior commissure, which was used to align the rostral-caudal sections from different animals.

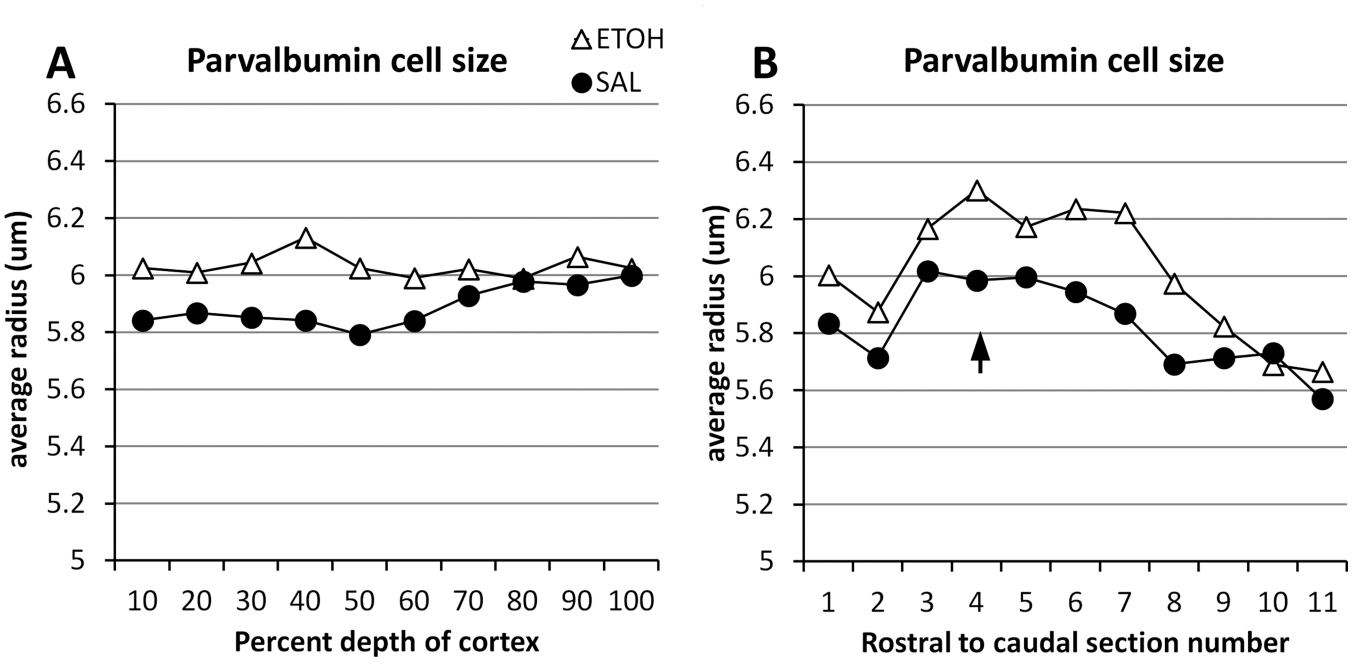

Figure 5.

Parvalbumin neuron size was slightly larger in the ethanol-treated animals. **A**. Separation of size measurements by depth of cortex showed that increased size was present mainly in the upper 60% of cortical depth. **B**. Separation of parvalbumin cell-size measurements by rostral-caudal sections indicated that this size difference was similar throughout neocortex.

Table 1

Compare groups									[a]Compare strains			[a]Compare sexes		
	SAL	[b]% C.V.	N	EtOH	% C.V.	N	Ratio ETOH/SAL	*p* value	SAL Ratio C57BL/ BALB/c	EtOH Ratio C57BL/ BALB/c		SAL Ratio male/ female	EtOH Ratio male/ female	
Body weight (g)	21.3	(13)	12	19.6	(14)	12	0.92	*	1.10	1.12	++	1.20	1.21	++
Brain volume (cm^3)														
MRI	0.47	(4)	11	0.42	(8)	12	0.90	***	1.01	1.08		1.02	0.98	
fluid displacement	0.41	(4)	12	0.36	(7)	12	0.87	***	0.98	1.02		0.98	0.97	
Cortex (both hemispheres)														
volume (mm^3)	60	(8)	12	53	(9)	12	0.88	**	1.01	1.12		1.00	1.03	
surface area (mm^2)	83	(5)	12	75	(6)	12	0.91	***	1.02	1.08		1.01	1.01	
thickness (μm)	900	(6)	12	870	(6)	12	0.97		0.99	1.07		1.03	1.02	
2-D neuron density(cells/mm^2)														
PV	248	(12)	10	202	(25)	12	0.81	***	0.81	0.73	++	0.79	0.80	++
CR	116	(16)	11	95	(14)	12	0.82	***	1.22	1.16	++	1.24	1.07	+
3-D neuron density (cells/$mm^3 \times 10^{-3}$)														
PV	10.4	(30)	6	7.3	(28)	6	0.71	**	--	--		0.58	0.64	++
CR	3.2	(7)	6	2.4	(10)	6	0.74	***	--	--		1.09	0.92	
NeuN	185	(5)	6	181	(9)	6	0.98		--	--		1.00	1.07	
Neuron number ($\times 10^{-3}$, left hemisphere only)														
PV	310	(25)	6	206	(27)	6	0.67	***	--	--		0.64	0.68	++
CR	98	(11)	6	68	(12)	6	0.69	***	--	--		1.21	0.97	
Neun	5,582	(8)	6	5,119	(11)	6	0.92	#	--	--		1.11	1.13	+
Neuron label density														
PV	34.9	(8)	6	33.1	(19)	6	0.95		--	--		0.92	0.87	
CR	44.2	(5)	6	43.8	(9)	6	0.99		--	--		1.03	1.14	
NeuN	30.5	(8)	6	29.4	(13)	6	0.96		--	--		0.92	1.10	
Neuron size (radius in microns)														
PV	5.9	(2)	6	6.0	(3)	6	1.03		--	--		1.01	0.99	

Compare groups									[a]Compare strains		[a]Compare sexes		
	SAL	[b]% C.V.	N	EtOH	% C.V.	N	Ratio ETOH/SAL	*p* value	SAL Ratio C57BL/ BALB/c	EtOH Ratio C57BL/ BALB/c	SAL Ratio male/ female	EtOH Ratio male/ female	
CR	5.1	(3)	6	5.1	(3)	6	1.00		--	--	1.05	1.06	++
NeuN	5.5	(2)	6	5.4	(5)	6	0.98		--	--	1.03	0.98	

[a]Values show ratios between strains or sexes within each treatment group.

[b]Percent coefficient of variation (% C.V.) = 100 × S.D./mean.

#$p < 0.1$,

*$p < 0.05$,

**$p < 0.01$,

***$p < 0.001$, for ANCOVA comparisons between treatment groups.

+$p < 0.05$,

++$p < 0.01$, for ANCOVA comparisons of strain or gender, using both SAL and EtOH animals.